Applied Mathematics & Information Sciences
An International Journal

http://dx.doi.org/10.18576/amis/140104

Effects of Slip Velocity and Hall Currents on Peristaltic Transport of Bingham-Papanastasiou Fluid with Heat Transfer

Nabil T. M. Eldabe[1], *Amira S. A. Asar*[2,3,*] *and Hameda M. Shawky*[3]

[1]Mathematics Department, Faculty of Education, Ain-Shams University, Cairo, Egypt
[2]Mathematics Department, Faculty of Arts & Science, Prince Sattam Bin Abdulaziz University, Wadi Adwassir, Saudi Arabia
[3]Mathematics Department, Faculty of Science (Girls), Al-Azhar University, Cairo, Egypt

Received: 2 Jun. 2019, Revised: 2 Oct. 2019, Accepted: 8 Oc. 2019
Published online: 1 Jan. 2020

Abstract: In this paper , we study the effects of slip boundary condition and Hall currents on peristaltic motion of a non-Newtonian fluid which follows Bingham-Papanastasiou model, with heat transfer taking into account the thermal radiation and heat generation, through an asymmetric channel. This phenomena is modeled mathematically by a system of governing equations which are continuity, momentum and heat equations. These equations are solved analytically under low Reynolds number condition and long wavelength approximation. The stream function and temperature distribution are obtained as functions of physical parameters of the problem. The effects of the parameters on these solutions are discussed numerically and illustrated graphically through a set of figures. It is found that the physical parameters have important roles to control the velocity and temperature distribution.

Keywords: Slip boundary condition; Hall currents; Peristaltic transport; Bingham-Papanastasiou fluid model; Thermal radiation; Heat generation.

1 Introduction

The word peristalsis stems from the Greek word peristalikos. Peristalsis is defined as a wave of relaxation contraction (expansion) imparted by the walls of a flexible conduit, thereby pumping the enclosed material, it is a nature's way of moving the content within hollow muscular structures by successive contraction of their muscular fibers [1,2,3,4]. Peristalsis is now well-known to the physiologists to be one of the major mechanisms for fluid transport in many biological systems, it results physiologically from neuron muscular properties of the tubular smooth muscles [5,6].

The peristaltic transport may be involved in many biological organs, e.g., swelling food through the esophagus, movement of chime in the gastrointestinal tract, urine transport from the kidney to the bladder through the ureter, transport of spermatozoa in the ducts efferent of male reproduction tract and in the cervical canal of the female, movement of ova in the fallopian tub, vasomotion of small blood vessels such as venules and capillaries as well as blood flow in arteries, and in many other glandular ducts [3,4,5,6,7]. There are also many industrial applications of the peristaltic transport like, blood pumps in heart lung machine, transport of corrosive fluid, where the contact of the fluid with the machinery parts is prohibited [4].

Although the majority of fluids in the biosphere have Newtonian behavior, non-Newtonian behavior is observed in most industrial synthetic and non-synthetic fluids and in biological fluids, such as human blood and saliva. To quote a few examples, crude oil and drilling muds from the oil industry, paints, cosmetics, glues, soaps, detergents and many food products. Among them, an important class of non-Newtonian materials presents a yield stress limit which must be exceeded before significant deformation can occur the so-called Viscoplastic materials. In order to model the stress-strain relation in these fluids, some fitting has been proposed such as the linear Bingham equation and the non-linear Herschel-Bulkley and Casson models [8,9,10].

On the other hand Viscoplastic fluids are characterized by the absence of deformations when the

* Corresponding author e-mail: amerasalem5@yahoo.com

applied load is below a fixed threshold. Bingham fluids is a special class of Viscoplatic fluids named so after Bingham [11], who described several types of paint using this definition. Viscoplastic fluids constitute a very important class of non-Newtonian fluids. The modelling of Bingham materials is of crucial importance in industrial applications, since a large variety of materials (e.g. foams, pastes, slurries, oils, ceramics, etc.) exhibit the fundamental character of viscoplasticity, that is the capability off lowing only if the stress is above some critical value [12,13,14].

However, the Bingham model is not amenable to numerical analysis because in some complex applications, parts of material flow while the rest behaves as a solid. This causes difficulties in tracking the shape and the location of the yield surfaces and applying two different constitutive equations across them. In addition, at vanishing shear rates, the apparent viscosity in Bingham model becomes infinite, which leads to a discontinuity and numerical difficulties. To overcome these issues, Papanastasiou proposed a modified Bingham model to approximate the rheological behavior of Bingham type materials [15,16,17].

We are aware that the no-slip condition in fluid mechanics means that the fluid velocity matches the velocity of the solid boundary. Nearly 200 years ago Navier proposed in his original paper on linearly viscous fluids a general boundary condition that permits the possibility of slip at a solid boundary. This boundary condition assumes that the tangential velocity of the fluid relative to the solid at a point on its surface is proportional to the tangential stress acting at that point. The constant of proportionality between these two quantities may be termed a coefficient of sliding friction (the slip parameter), which is assumed to depend on the nature of the fluid and the solid surface [18]. Some experimental and theoretical studies stated that slip condition could not be ruled out as an important element to understanding of certain characteristic flow [19].

The fluid flows in the presence of magnetic field has promising applications in engineering, chemistry, physics, the polymer industry and metallurgy. Some examples include controlling the rate of cooling, blood plasma, drying, evaporation at the surface of a water body, geothermal reservoirs, thermal insulation, enhanced oil recovery, cooling of nuclear reactors, bleeding reduction during surgeries, hyperthermia etc. Also under the influence of powerful applied magnetic fields the Hall effects in peristalsis cannot be ignored. In such case the applied magnetic field is powerful or collision frequency is small [20].

There are several studies of peristaltic transport with different fluids under the effect of different types of the external forces, as mentioned in [21] and see also, [22,23, 24]. To the best of our knowledge, no investigation has been made yet to investigate the effect of slip velocity on peristaltic transport for Bingham-Papanastasiou fluid in the presence of Hall current and heat transfer.

In this article the vector form of the equations of motion of the non-Newtonian Bingham-Papanastasiou fluid as well as energy equation and the constitutive equations of that fluid are written in section 2. The formulation of the problem is introduced mathematically in section 3. In section 4 the stream, velocity and temperature distribution functions; which are calculated analytically and with the help of Mathematica program; are written. Results and discussion are explained in section 5 and the conclusion in section 6, this paper ends by the appendix and list of references.

2 Vector form of the problem's equations

The basic equations which describe the motion of non-Newtonian fluid with heat transfer can be written as

Continuity equation

$$\nabla \cdot \underline{V} = 0, \tag{1}$$

Momentum equation

$$\rho \frac{d\,\underline{V}}{dt} = -\nabla P + \nabla \cdot \underline{S} + \underline{J} \wedge \underline{B} \tag{2}$$

Energy equation

$$\rho c_p \frac{d\,T}{dt} = k_1 \nabla^2 T + \underline{S} \cdot \nabla\, \underline{V} - \nabla \cdot \underline{q_r} + Q(T - T_0), \tag{3}$$

where

$$\underline{J} = \sigma \left[(\underline{V} \wedge \underline{B}) - \frac{1}{e\, n_e} (\underline{J} \wedge \underline{B}) \right],$$

$\underline{V}$ is fluid velocity vector, ρ is the density of the fluid, P is the pressure, $\underline{S}$ is the extra-stress tensor (S_{ij}), $\underline{J}$ is the current density vector including the Hall effect, σ is the electric conductivity, e is the electric charge, n_e is the number density of electrons, $\underline{B} = (0,0,B_0)$ is the uniform magnetic field with magnetic flux density, T is temperature, k_1 is the thermal conductivity, $\frac{d}{dt}$ denotes the material time derivative and ∇^2 is the Laplacian operator, Q is heat generation, $\underline{q_r}$ the radiation heat flux vector.

The regularized constitutive equation proposed by Papanastasiou [25] is

$$\underline{S} = \left[\mu + \frac{S_0(1 - \exp(-m\dot{\gamma}))}{\dot{\gamma}} \right] \underline{\dot{\gamma}}, \tag{4}$$

where μ is the plastic viscosity, S_0 is the yield stress, m is a stress growth exponent and $\underline{\dot{\gamma}}$ denotes the rate of strain tensor;

$$\underline{\dot{\gamma}} = \nabla\, \underline{V} + (\nabla\, \underline{V})^{\mathrm{T}} \tag{5}$$

($\nabla \underline{V}$ is the velocity-gradient tensor and $(\nabla \underline{V})^{\mathrm{T}}$ is its transpose) and $\dot{\gamma}$ is the magnitude of the rate of strain tensor,

$$\dot{\gamma} = |\underline{\dot{\gamma}}| = \sqrt{\frac{1}{2} II_{\underline{\dot{\gamma}}}} = \sqrt{\frac{1}{2} \underline{\dot{\gamma}} : \underline{\dot{\gamma}}} = \sqrt{\frac{1}{2} \sum_i \sum_j \dot{\gamma}_{ij} \dot{\gamma}_{ji}}\,, \quad (6)$$

where $II_{\underline{\dot{\gamma}}}$ is the second invariant of $\underline{\dot{\gamma}}$.

3 Mathematical formulation

Consider flow of fluid in two-dimensional asymmetric channel, X-axis is taken in motion direction while Y-axis is perpendicular on it and (U,V) are the velocity components in X and Y directions respectively as shown in Fig.(1).

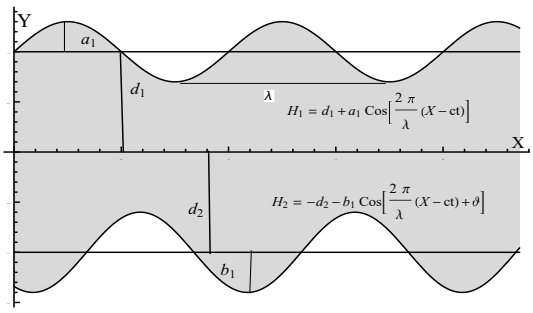

Fig. 1: The geometry of the problem.

The channel asymmetry is produced by choosing the peristaltic wave train on the walls to have different amplitudes and phase, consider the upper and lower channel walls are

$$Y = H_1 = d_1 + a_1 \cos\left[\frac{2\pi}{\lambda}(X - c\,t)\right] \quad (7)$$

$$Y = H_2 = -\,d_2 - \,b_1 \cos\left[\frac{2\pi}{\lambda}(X - c\,t) + \vartheta\right] \quad (8)$$

where a_1 and b_1 are the amplitudes of the waves, λ is the wavelength, $(d_1 + d_2)$ is the width of the channel and ϑ is the phase difference that varies in the range $0 \le \vartheta \le \pi$. Further, a_1, b_1, d_1, d_2 and ϑ satisfy the condition $a_1^2 + b_1^2 + 2a_1 b_1 \cos\vartheta \le (d_1 + d_2)^2$.

Introducing a wave frame (x,y) moving with the velocity c away from the laboratory frame (X,Y), by the transformations

$$x = X - c\,t, \quad y = Y, \quad u = U - c, \quad v = V, \quad p\,(x) = P(X,t), \quad (9)$$

where u and v are the fluid velocity components and p is pressure in the wave frame of references.

Equations (1-3) will be on the form

$$\frac{\partial u}{\partial x} + \frac{\partial v}{\partial y} = 0, \quad (10)$$

$$u\frac{\partial u}{\partial x} + v\frac{\partial u}{\partial y} = -\frac{1}{\rho}\frac{\partial P}{\partial x} + \frac{\partial S_{xx}}{\partial x} + \frac{\partial S_{xy}}{\partial y} + \frac{\sigma B_0^2}{1+\mathbf{H}^2}(\mathbf{H}v - (u+c)), \quad (11)$$

$$u\frac{\partial v}{\partial x} + v\frac{\partial v}{\partial y} = -\frac{1}{\rho}\frac{\partial P}{\partial y} + \frac{\partial S_{yx}}{\partial x} + \frac{\partial S_{yy}}{\partial y} - \frac{\sigma B_0^2}{1+\mathbf{H}^2}(v + \mathbf{H}(u+c)), \quad (12)$$

$$\rho c_p \left(u\frac{\partial T}{\partial x} + v\frac{\partial T}{\partial y}\right) = k_1 \left(\frac{\partial^2 T}{\partial x^2} + \frac{\partial^2 T}{\partial y^2}\right) + S_{xx}\frac{\partial u}{\partial x} + S_{xy}\frac{\partial u}{\partial y} + S_{yx}\frac{\partial v}{\partial x} + S_{yy}\frac{\partial v}{\partial y} - \frac{\partial q_r}{\partial y} + Q(T - T_0), \quad (13)$$

where $\mathbf{H} = \frac{\sigma B_0}{e\,n_e}$ is the Hall parameter and the radiative heat flux in the $X-$ direction is considered as negligible compared to $Y-$ direction.

Also, the constitutive equations become

$$S_{xx} = 2\left(\mu + \frac{S_0}{\dot{\gamma}}\left(1 - e^{-m\dot{\gamma}}\right)\right)\frac{\partial u}{\partial x}, \quad (14)$$

$$S_{xy} = S_{yx} = \left(\mu + \frac{S_0}{\dot{\gamma}}\left(1 - e^{-m\dot{\gamma}}\right)\right)\left(\frac{\partial u}{\partial y} + \frac{\partial v}{\partial x}\right), \quad (15)$$

$$S_{yy} = 2\left(\mu + \frac{S_0}{\dot{\gamma}}\left(1 - e^{-m\dot{\gamma}}\right)\right)\frac{\partial v}{\partial y}, \quad (16)$$

with

$$\dot{\gamma} = \left[2\left(\frac{\partial u}{\partial x}\right)^2 + \left(\frac{\partial u}{\partial y} + \frac{\partial v}{\partial x}\right)^2 + 2\left(\frac{\partial v}{\partial y}\right)^2\right]^{\frac{1}{2}}, \quad (17)$$

and the wall equations will be

$$y = d_1 + a_1 \cos\frac{2\pi}{\lambda}x \quad (18)$$

$$y = -\,d_2 - \,b_1 \cos\left[\frac{2\pi}{\lambda}x + \vartheta\right]. \quad (19)$$

Further, by using Rosseland approximation for radiation, the radiative heat flux q_r is given by

$$q_r = -\frac{4}{3}\frac{\sigma_0}{k_0}\frac{\partial T^4}{\partial Y}$$

where σ_0 is Stefan-Boltzman constant and k_0 is the Rosseland mean absorption coefficient.

Moreover, we suppose that the temperature difference within the flow is sufficiently small such that T^4 may be expanded in a Taylor series. Hence, expanding T^4 about T_0 and ignoring higher order terms we get:

$$T^4 \cong 4\,T_0^3\,T - 3\,T_0^4$$

i.e

$$q_r = -\frac{16}{3}\frac{\sigma_0 T_0^3}{k_0}\frac{\partial T}{\partial Y} \tag{20}$$

Now introducing the stream function ψ ($u = \frac{\partial \psi}{\partial y}, v = -\frac{\partial \psi}{\partial x}$) and the following non-dimensional variables

$$\bar{x} = \frac{x}{\lambda}, \bar{y} = \frac{y}{d_1}, \delta = \frac{d_1}{\lambda}, \bar{u} = \frac{u}{c}, \bar{v} = \frac{v}{\delta c}, \bar{t} = \frac{c\,t}{\lambda}, a = \frac{a_1}{d_1},$$

$$b = \frac{b_1}{d_1}, d = \frac{d_2}{d_1}, h_1 = \frac{H_1}{d_1}, h_2 = \frac{H_2}{d_1}, \bar{\psi} = \frac{\psi}{c\,d_1}, \bar{S} = \frac{d}{\mu c} S$$

$$\bar{\dot{\gamma}} = \frac{d_1\,\dot{\gamma}}{c}, \bar{p} = \frac{d_1^2\,p}{\mu\,\lambda\,c}, R = \frac{\rho c\,d_1}{\mu}, \mathscr{K} = \frac{\sigma B_0^2 d_1^2}{\mu}, \Theta = \frac{T - T_0}{T_w - T_0}, \tag{21}$$

after dropping bars and under the assumptions of long wavelength ($\delta \ll 1$) and low Reynolds number, the equation of continuity is simply verified.

Equations (11 - 13), using equation (20), become

$$-\frac{\partial p}{\partial x} + \frac{\partial S_{xy}}{\partial y} - \mathscr{H}^2\left(\frac{\partial \psi}{\partial y} + 1\right) = 0 \tag{22}$$

$$\frac{\partial p}{\partial y} = 0, \tag{23}$$

$$\left(1 + \frac{4}{3R_n}\right)\frac{\partial^2 \Theta}{\partial y^2} + P_r\,G\,\Theta + P_r\,E_c\,S_{xy}\frac{\partial^2 \psi}{\partial y^2} = 0, \tag{24}$$

Also, equations (14 - 17) become

$$S_{xx} = 0 \tag{25}$$

$$S_{xy} = \left[1 + \frac{B_n}{|\dot{\gamma}|}\left(1 - e^{-M|\dot{\gamma}|}\right)\right]\left(\frac{\partial^2 \psi}{\partial y^2}\right), \tag{26}$$

$$S_{yy} = 0 \tag{27}$$

$$|\dot{\gamma}| = \frac{\partial^2 \psi}{\partial y^2}. \tag{28}$$

So we can write

$$S_{xy} = \left[1 + \frac{B_n}{|\dot{\gamma}|}\left(1 - e^{-M|\dot{\gamma}|}\right)\right]\frac{\partial^2 \psi}{\partial y^2} \tag{29}$$

and for small values of M we will get

$$S_{xy} = (1 + B_n M)\frac{\partial^2 \psi}{\partial y^2} \tag{30}$$

where $\mathscr{H}^2 = \frac{\mathscr{K}}{1+\mathbf{H}^2}$, $E_c = \frac{\mu c^2}{k_1 \Delta T} = \frac{c^2}{c_p \Delta T}$ is the Eckert number, $B_n = \frac{d_1}{\mu c} S_0$ is Bingham number, $M = \frac{c\,m}{d_1}$ is the dimensionless stress growth exponent, $P_r = \frac{\mu C_p}{k_1}$ is the Prantdel number, $R_n = \frac{k_1 k_0}{4\sigma_0 T_0^3}$ is the radiation parameter, $G = \frac{Q d_1^2}{\mu C_p}$ is the generation parameter.

Equation (23) implies that $p \neq p(y)$, so we can write equation (24) after using (30) on the form

$$\left[\frac{\partial^2}{\partial y^2} - \frac{\mathscr{H}^2}{(1 + B_n M)}\right]\frac{\partial^2 \psi}{\partial y^2} = 0 \tag{31}$$

also, equation (24) will take the form

$$\left(1 + \frac{4}{3R_n}\right)\frac{\partial^2 \Theta}{\partial y^2} + P_r\,G\,\Theta + P_r\,E_c(1 + B_n M)\left(\frac{\partial^2 \psi}{\partial y^2}\right)^2 = 0 \tag{32}$$

It is obvious that when $B_n = 0$ equations (31) and (32) will represent the equations of motion and energy of ordinary Newtonian fluid.

Furthermore, the upper and lower channel walls in dimensionless forms will be

$$y = h_1 = 1 + a\,\cos 2\pi x, \tag{33}$$

$$y = h_2 = -d - b\,(\cos 2\pi x + \vartheta). \tag{34}$$

Also, the non-dimensional appropriate boundary conditions will be

$$\psi = \frac{q}{2}, \quad \frac{\partial \psi}{\partial y} + \beta\,\frac{\partial^2 \psi}{\partial y^2} = -1, \quad \Theta = 1, \quad at\ y = h_1, \tag{35}$$

$$\psi = -\frac{q}{2}, \quad \frac{\partial \psi}{\partial y} - \beta\,\frac{\partial^2 \psi}{\partial y^2} = -1, \quad \Theta = 0, \quad at\ y = h_2, \tag{36}$$

where q is the flux between the two walls in the wave frame and β is the non-dimensional slip parameter.

q is related to the dimensionless average volume flow rate over one period $T = \frac{\lambda}{c}$ of the peristaltic wave in the laboratory frame $\overline{Q}$ through the relation $\overline{Q} = q + d + 1$.

Also, by integrating the axial pressure gradient $\frac{dp}{dx}$ over one wavelength λ, the pressure rise is given by the relation

$$\Delta p = \int_0^1 \frac{dp}{dx} dx \tag{37}$$

4 The proposed solution of the problem

Through introducing the boundary conditions (35 -36) into (31, 32) the stream function will be

$$\begin{aligned}\psi = [&l_7\,(h_1 + h_2 - 2y) + 2\,(l_8 \sinh\alpha\,(y - h_1) \\ &+ l_9 \cosh\alpha\,(y - h_1) + h_1 - 2y) \\ &+ 2\,(l_{10}\sinh\alpha\,(y - h_2) + l_{11}\cosh\alpha\,(y - h_2) - h_2)]\,l_{12}\end{aligned}$$

so the velocity in x-direction will be

$$u = [-2l_7 + 2(l_8\alpha\cosh\alpha(y-h_1) + l_9\alpha\sinh\alpha(y-h_1) - 2) + 2(l_{10}\alpha\cosh\alpha(y-h_2) + l_{11}\alpha\sinh\alpha(y-h_2))]l_{12}$$

and the temperature distribution equation will be

$$\Theta = l_{14}(\alpha^4K^2E_cl_{11}^2(3R_n(4\alpha^2 - GP_r\times (\cosh\alpha(-h_1-h_2+2y)-1)) + 16\alpha^2)) + A_1\sinh(\zeta y) + A_2\cosh(\zeta y)$$

Where $\alpha, \zeta, l_1 - l_{14}, A_1$ andA_2 are given in the Appendix.

5 Results and discussion

In this section, we have presented a set of Figures (2-21), that describe qualitatively the effects of various parameters of interest on flow quantities such as the axial velocity u, axial pressure gradient $\frac{dp}{dx}$, pressure rise per wavelength ΔP, temperature distribution Θ.

Figs. (2-5) illustrate the variation of axial pressure gradient $\frac{dp}{dx}$ with x for different values of Bingham number B_n, slip parameter β and Hall parameter $\mathbf{H}$. The following results can be observed from these figures, the magnitude of the pressure gradient increases with increasing of B_n as shown in Fig. (2), while Figs. (3,4) showed that the magnitude of the pressure gradient decreases with increasing both of β and $\mathbf{H}$. It is also observed that the maximum pressure gradient occurs at the narrow part of the channel $x \simeq 0.42$, while in the special case of symmetric channel (a=b,$\vartheta = 0$) the narrow part at which the pressure gradient is maximum will be $x = 0.5$ (the middle of distance $x = 1$) as shown in Fig. (5) and that will be proved if we studied the effects of all parameters on $\frac{dp}{dx}$ for symmetric channel.

The effects of the phase angle ϑ, B_n, β and $\mathbf{H}$ on the variation of the pressure rise ΔP with the average volume flow rate $\overline{Q}$ are illustrated in Figs. (6-9). By looking at those figures, it is noticeable that ΔP has the maximum value when $\overline{Q}$ is minimum and ΔP decreases until it has the minimum value when $\overline{Q}$ is maximum. It is observed from Fig. (6) that the pressure rise decreases with the increasing of ϑ.

From Fig. (7), it is obvious that the pressure rise increases with B_n in region above a critical point (at which there no noticeable difference) and after that point it is obvious that the contrary occurs and ΔP decreases with the increasing in B_n.

Figs. (8,9) explain the effect of β and $\mathbf{H}$, it is clear that ΔP decreases with the increasing in β and $\mathbf{H}$ in the region above a critical point and after that point we notice that ΔP increases with decreasing in β and $\mathbf{H}$.

Figs. (10-17) illustrat the effects of B_n, $\mathbf{H}$, β, ϑ, Eckert number E_c, generation parameter G, Prantdel P_r and radiation parameter R_n on the temperature Θ. In Figs. (10-16) we consider that $a = 0.5$, $b = 0.3$, $d = 0.5$, $x = 1$, $\vartheta = \frac{\pi}{2}$, i.e $= h_1 = -1, h_2 = 1.5$. It is obvious that the temperature distribution satisfies our boundary conditions where $\Theta = 0$ at $y = h_1 = -1$ and $\Theta = 1$ at $y = h_2 = 1.5$. We observe that Θ increases with B_n, E_c, G, $\mathbf{H}$, P_r and R_n as shown in Figs. (10-15). From Fig. (16) it is clear that Θ decreases in the increase of the slip parameter β.

Fig. (17) clarifies the effect of ϑ on the temperature distribution, it is obvious that Θ decreases with the increasing of ϑ. Also our boundary conditions on Θ are fulfilled where $\Theta = 1$ at $y = h_2 = 1.5$ for all values of ϑ and $\Theta = 0$: at $y = h_1 = -1.3$ when $\vartheta = 0$, at $y = h_1 \simeq -1.21$ when $\vartheta = \frac{\pi}{4}$ and at $y = h_1 = -1$ when $\vartheta = \frac{\pi}{2}$.

Figures (18-21) explain the effect of some parameters of the problem on the velocity distribution u. We observe that u increases with B_n, $\mathbf{H}$ and ϑ as cleared through Figs. (18-20), while u decreases with increasing of the slip parameter β as illustrated in Fig. (21).

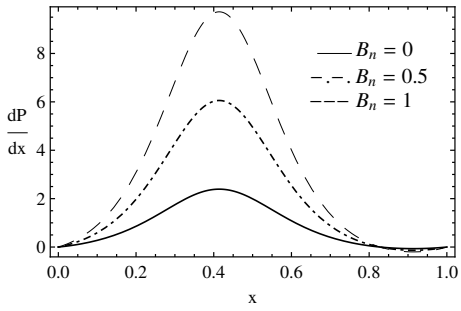

Fig. 2: The variation of the pressure gradient $\frac{dp}{dx}$ with x for several values of B_n when $a = 0.5$, $b = 0.3$, $d = 1$, $\vartheta = \frac{\pi}{2}$, $\overline{Q} = -0.5$, $\mathscr{K} = 1.2$, $\beta = 0.5$, $\mathbf{H} = 0.1$, $M = 5$.

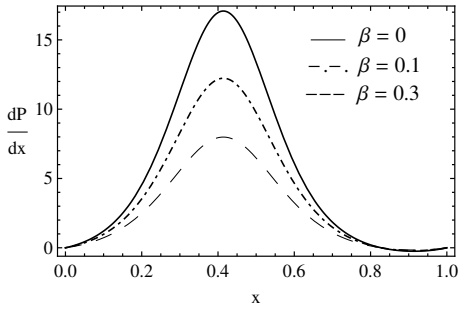

Fig. 3: The variation of the pressure gradient $\frac{dp}{dx}$ with x for several values of β when $a = 0.5$, $b = 0.3$, $d = 1$, $\vartheta = \frac{\pi}{2}$, $\overline{Q} = -0.5$, $\mathscr{K} = 1.2$, $B_n = 0.5$, $\mathbf{H} = 0.1$, $M = 5$.

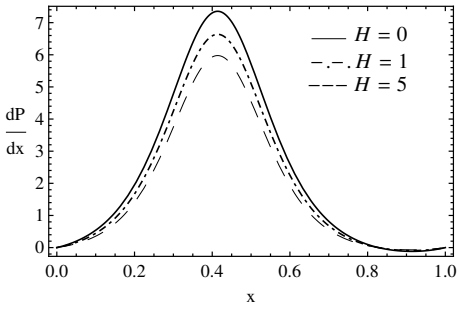

Fig. 4: The variation of the pressure gradient $\frac{dp}{dx}$ with x for several values of H when $a = 0.5$, $b = 0.3$, $d = 1$, $\vartheta = \frac{\pi}{2}$, $\overline{Q} = -0.5$, $\mathscr{K} = 1.2$, $\beta = 0.5$, $\mathbf{H} = 0.1$, $B_n = 0.5$, $M = 5$.

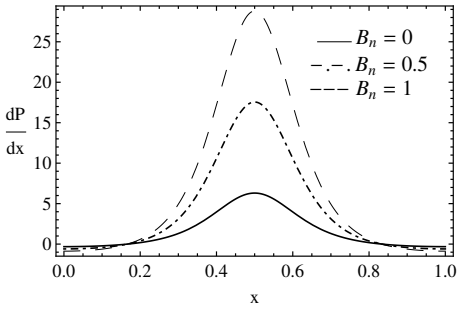

Fig. 5: The variation of the pressure gradient $\frac{dp}{dx}$ with x for several values of B_n when $a = 0.5$, $b = 0.5$, $d = 1$, $\vartheta = 0$, $\overline{Q} = -0.5$, $\mathscr{K} = 1.2$, $\beta = 0.5$, $\mathbf{H} = 0.1$, $M = 5$.

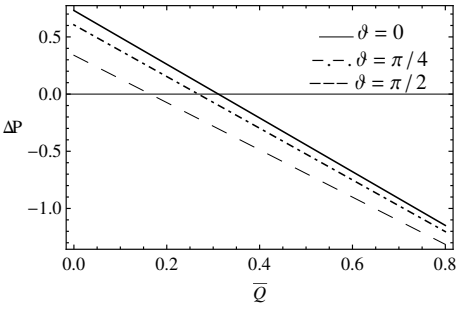

Fig. 6: The variation of the pressure rise ΔP with $\overline{Q}$ for several values of ϑ when $a = 0.5$, $b = 0.3$, $d = 1$, $\mathscr{K} = 1.2$, $\beta = 0.5$, $\mathbf{H} = 0.1$, $B_n = 0.2$, $M = 5$.

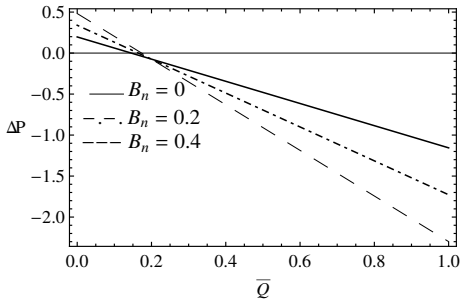

Fig. 7: The variation of the pressure rise ΔP with $\overline{Q}$ for several values of B_n when $a = 0.5$, $b = 0.3$, $d = 1$, $\vartheta = \frac{\pi}{2}$, $\mathscr{K} = 1.2$, $\beta = 0.5$, $\mathbf{H} = 0.1$, $M = 5$.

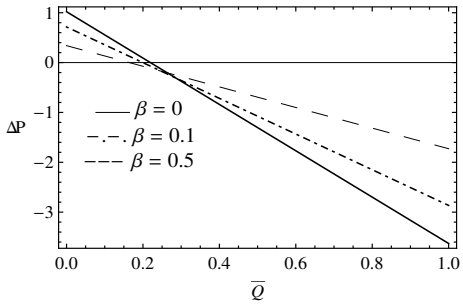

Fig. 8: The variation of the pressure rise ΔP with $\overline{Q}$ for several values of β when $a = 0.5$, $b = 0.3$, $d = 1$, $\vartheta = \frac{\pi}{2}$, $\mathscr{K} = 1.2$, $\mathbf{H} = 0.1$, $B_n = 0.2$, $M = 5$.

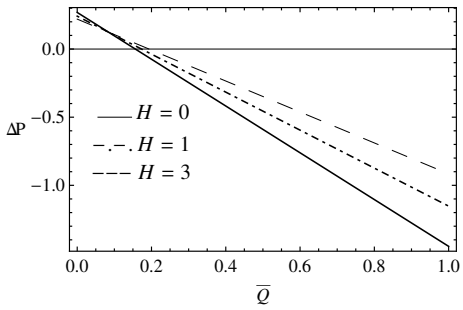

Fig. 9: The variation of the pressure rise ΔP with $\overline{Q}$ for several values of $\mathbf{H}$ when $a = 0.5$, $b = 0.3$, $d = 1$, $\vartheta = \frac{\pi}{2}$, $\mathscr{K} = 1.2$, $\beta = 0.5$, $B_n = 0.1$, $M = 5$.

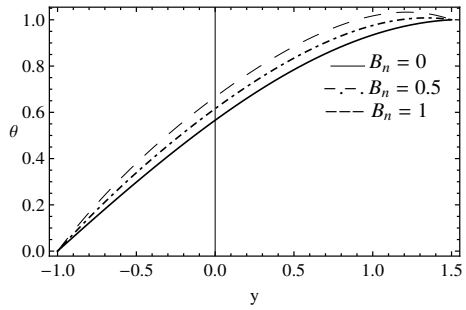

Fig. 10: The temperature distribution Θ is plotted against y for different values of Bingham number B_n when $a = 0.5$, $b = 0.3$, $d = 1$, $x = 1$, $\vartheta = \frac{\pi}{2}$, $q = 0.5$, $\mathscr{K} = 1.2$, $\beta = 0.5$, $\mathbf{H} = 0.1$, $M = 10$, $E_c = 0.1$, $P_r = 0.5$, $R_n = 3$, $G = 1$.

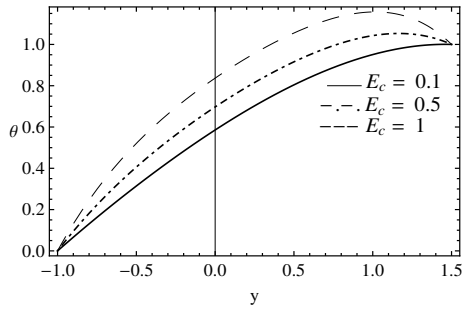

Fig. 11: The temperature distribution Θ is plotted against y for different values of Eckert number E_c when $a = 0.5$, $b = 0.3$, $d = 1$, $x = 1$, $\vartheta = \frac{\pi}{2}$, $q = 0.5$, $\mathscr{K} = 1.2$, $\beta = 0.5$, $\mathbf{H} = 0.1$, $M = 10$, $B_n = 0.2$, $P_r = 0.5$, $R_n = 3$, $G = 1$.

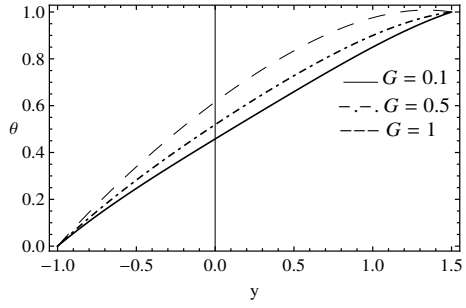

Fig. 12: The temperature distribution Θ is plotted against y for different values of heat generation parameter G when $a = 0.5$, $b = 0.3$, $d = 1$, $x = 1$, $\vartheta = \frac{\pi}{2}$, $q = 0.5$, $\mathscr{K} = 1.2$, $\beta = 0.5$, $\mathbf{H} = 0.1$, $M = 10$, $B_n = 0.5$, $P_r = 0.5$, $R_n = 3$, $E_c = 0.1$.

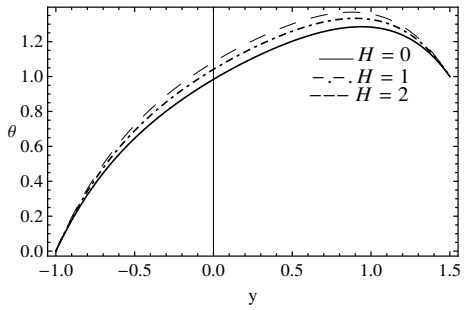

Fig. 13: The temperature distribution Θ is plotted against y for different values of Hall parameter $\mathbf{H}$ when $a = 0.5$, $b = 0.3$, $d = 1$, $x = 1$, $\vartheta = \frac{\pi}{2}$, $q = 0.5$, $\mathscr{K} = 15$, $\beta = 0.5$, $E_c = 0.5$, $M = 10$, $B_n = 1$, $P_r = 0.5$, $R_n = 3$, $G = 1$.

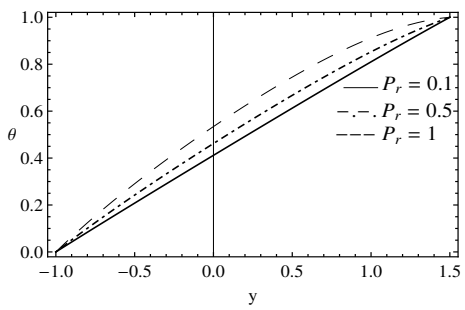

Fig. 14: The temperature distribution Θ is plotted against y for different values of the Prantdel number P_r when $a = 0.5$, $b = 0.3$, $d = 1$, $x = 1$, $q = 0.5$, $\vartheta = \frac{\pi}{2}$, $\mathscr{K} = 1.2$, $\beta = 0.5$, $E_c = 0.1$, $M = 10$, $\mathbf{H} = 0.1$, $B_n = 0.2$, $R_n = 3$, $G = 0.3$.

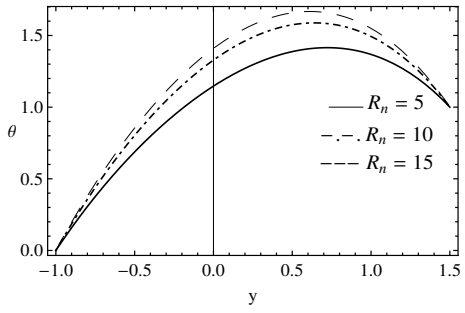

Fig. 15: The temperature distribution Θ is plotted against y for different values of the radiation parameter R_n when $a = 0.5$, $b = 0.3$, $d = 1$, $x = 1$, $q = 0.5$, $\vartheta = \frac{\pi}{2}$, $\mathscr{K} = 1.2$, $\beta = 0.5$, $E_c = 0.1$, $M = 10$, $\mathbf{H} = 0.1$, $B_n = 0.2$, $P_r = 3$, $G = 0.3$.

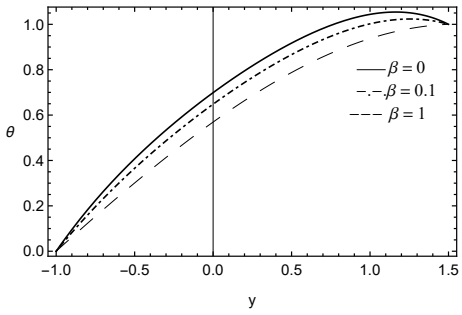

Fig. 16: The temperature distribution Θ is plotted against y for different values of the slip parameter β when $a = 0.5$, $b = 0.3$, $d = 1, x = 1, q = 0.5, \vartheta = \frac{\pi}{2}, \mathscr{K} = 1.2, R_n = 3, E_c = 0.1, M = 10,$ $\mathbf{H} = 0.1, B_n = 1, P_r = 0.5, G = 1$

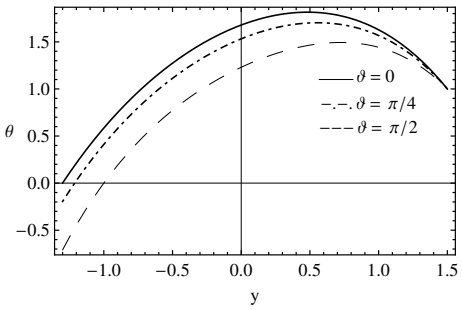

Fig. 17: The temperature distribution Θ is plotted against y for different values of the phase angle ϑ when $a = 0.5$, $b = 0.3$, $d = 1, x = 1, q = 0.5, \mathscr{K} = 1.2, \beta = 0.5, E_c = 0.1, M = 10, \mathbf{H} = 0.1,$ $B_n = 0.5, P_r = 3, R_n = 3, G = 0.3$.

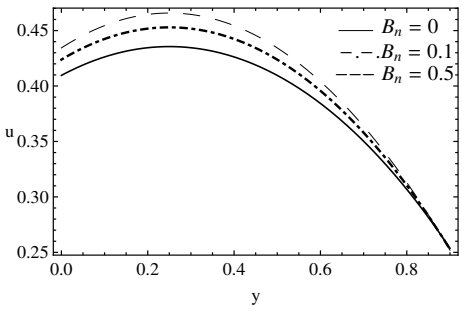

Fig. 18: The velocity u is plotted against y for different values of the Bingham number B_n when $a = 0.5$, $b = 0.3$, $d = 1$, $x = 1$, $q = 0.5$, $\vartheta = \frac{\pi}{2}$, $\beta = 0.5$, $\mathscr{K} = 1.2$, $M = 10$, $\mathbf{H} = 0.2$.

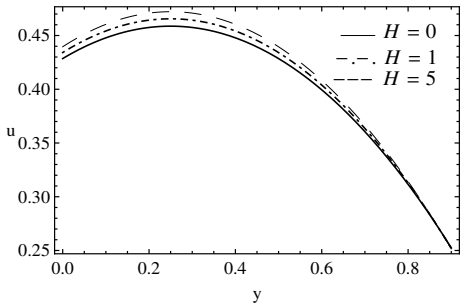

Fig. 19: The velocity u is plotted against y for different values of the Hall parameter $\mathbf{H}$ when $a = 0.5$, $b = 0.3$, $d = 1$, $x = 1$, $q = 0.5$, $\vartheta = \frac{\pi}{2}$, $\beta = 0.5$, $\mathscr{K} = 1.2$, $M = 10$, $B_n = 0.2$.

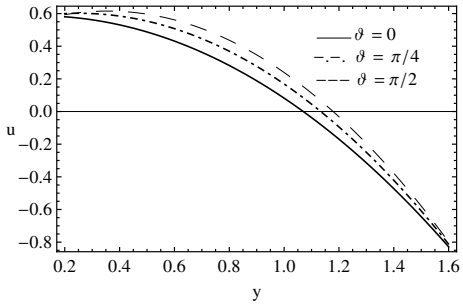

Fig. 20: The velocity u is plotted against y for different values of the phase angle ϑ when $a = 0.5$, $b = 0.3$,$d = 1$, $x = 1$, $q = 0.5$, $M = 10$, $\beta = 0.2$, $\mathscr{K} = 1.2$, $\mathbf{H} = .2$, $B_n = 5$.

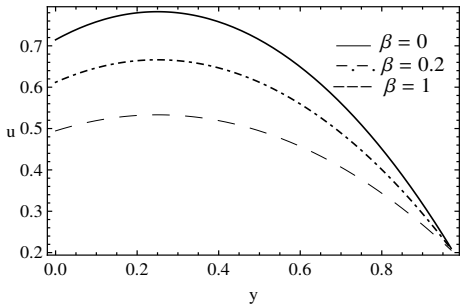

Fig. 21: The velocity u is plotted against y for different values of the slip parameter β when $a = 0.5$, $b = 0.3$, $d = 1$, $x = 1$, $q = 0.5$, $\vartheta = \frac{\pi}{2}$, $M = 10$, $\mathscr{K} = 1.2$, $\mathbf{H} = 1$, $B_n = 0.2$.

6 Conclusion

The problem of two-dimensional peristaltic flow of a non-Newtonian Bingham-Papanastasiou fluid with heat transfer, through asymmetric channel, under the influence of slip boundary condition and Hall currents is formed. The equations governing this motion have been solved analytically under the conditions of low Reynolds number and long wavelength approximations, subjected to a set of appropriate boundary conditions. The expressions of velocity and temperature distribution have been evaluated for different parameters and have been shown graphically through a set of figures. The very important results can be summarized as following:

1-the pressure gradient has the maximum value at $x \simeq 0.42$.

2-the pressure rise is maximum if the flow rate is minimum while it be minimum if the flow rate is maximum.

3-the temperature distribution increases with B_n, $\mathbf{H}$, E_c, G, P_r and R_n while it decreases with the increasing of β and ϑ.

4-the velocity increases with B_n, $\mathbf{H}$ and ϑ while it decreases with the increasing of the β.

Appendix

$$\alpha = \frac{\mathscr{H}}{\sqrt{(1+B_nM)}}, \quad \zeta = \sqrt{\frac{3GR_nP_r}{-3R_n-4}}, \quad l_1 = \frac{\alpha}{2}(h_1-h_2),$$
$$l_2 = 2\alpha\left((h_1-h_2)\left(\alpha^2\beta^2+1\right)-2\beta\right),$$

$$l_3 = 4\left(\alpha^2\beta(h_1-h_2)-1\right), \quad l_4 = l_2\sinh 2l_1 + l_3\cosh 2l_1 + 4, \quad l_5 = -\alpha\left(q\alpha^2\beta^2+2\beta+q\right), \quad l_6 = -2\left(q\alpha^2\beta+1\right),$$

$$l_7 = l_5\sinh 2l_1 + l_6\cosh 2l_1, \quad l_8 = -\alpha\beta(h_1+h_2+q), \quad l_9 = (h_1+h_2+q), \quad l_{10} = \alpha\beta(h_1-h_2+q),$$

$$l_{11} = (h_1-h_2+q), \quad l_{12} = \frac{1}{l_4}, \quad l_{14} = \frac{1}{l_{13}}, \quad l_{13} = 8G((\alpha\beta l_1-1)\sinh l_1 + l_1\cosh l_1))^2\left(3R_n(GP_r+4\alpha^2)+16\alpha^2\right),$$

$$A_1 = l_{14}[\mathrm{cosech}(\zeta(h_1-h_2))(\alpha^4K^2A_c\, l_{11}^2(\cosh(h_1\zeta)-\cosh(h_2\zeta))(3R_n(4\alpha^2-GP_r(\cosh(2l_1)-1))+16\alpha^2) + l_{13}\cosh(h_2\zeta)],$$

$$A_2 = -l_{14}[\mathrm{cosech}(\zeta(h_1-h_2))(\alpha^4K^2A_c\, l_{11}^2(\sinh(h_1\zeta)+\sinh(h_2\zeta))(3R_n(4\alpha^2-GP_r(\cosh(-2l_1)-1))+16\alpha^2)) + l_{13}\sinh(h_2\zeta)].$$

References

[1] O. Eytan, A.J. Jaffa, and D. Elad, *Peristaltic flow in a tapered channel: application to ambryo transport within the uterine cavity*, Med. Eng. and Phys., 23, 473-482(2001).

[2] Y.C. Fung, and C.S. Yih, *Peristaltic transport*, J. Applied Mechanics, 35, 669-675(1968).

[3] Kh.S. Mekheimer, *Nonlinear peristaltic transport through a porous medium in an inclined planar channel*, J. Porous Media, 6(3), 189-201(2003) .

[4] M. Mishra, and A.R. Rao, *Peristaltic transport of a Newtonian fluid in an asymmetric channel*, Z. angew. Math. Phys., 54, 532-550(2003).

[5] E.F. El-Shehawey, N.T. Eldabe, E.M. El-ghzey, and A. Ebaid, *Peristaltic transport in an asymmetric channel through a porous medium*, Applied Math. and Computation, 182, 140-150(2006).

[6] L.M. Srivastava, and V.P. Srivastava, *Peristaltic transport of a two-layered model of physiological fluid*, J. Biomech., 15(4), 257-265(1982).

[7] E.F. El-Shehawey and S.Z.A. Husseny, *Effects of porous boundaries on peristaltic transport through a porous medium*, Acta Mech., 143, 165-177(2000).

[8] G.H.R. Kefayati, and R.R. Huilgol, *Lattice Boltzmann Method for simulation of mixed convection of a Bingham fluid in a lid-driven cavity*, International Journal of Heat and Mass Transfer, 103, 725-743(2016).

[9] H.P. Soto, M.L. Martins-Costa, C. Fonseca, and S. Frey, *A Numerical Investigation of Inertia Flows of Bingham-Papanastasiou Fluids by an Extra Stress-Pressure-Velocity Galerkin Least-Squares Method*, J. of the Braz. Soc. of Mech. Sci. and Eng., 33(5), 450 -460(2010).

[10]P. Thakur, Sh. Mittal,, N. Tiwari, and R.P. Chhabra, *The motion of a rotating circula rcylinder in a stream of Bingham plastic fluid*, Journal of Non-Newtonian Fluid Mechanics, 235, 29-46(2016).

[11]E.C. Bingham, *An investigation of the laws of plastic flow*, Bulletin of the Bureau of Standards, 13, 309-353(1916).

[12]Y. Dimakopoulos, M. Pavlidis, and J. Tsamopoulos, *Steady bubble rise in Herschel-Bulkley fluids and comparison of predictions via the Augmented Lagrangian Method with those via the Papanastasiou model*, Journal of Non-Newtonian Fluid Mechanics, 200, 34-51(2013).

[13]L. Fusi, and A. Farina, *Flow of a Bingham fluid in a non symmetric inclined channel*, Journal of Non-Newtonian Fluid Mechanics, 238, 24-32(2016).

[14]O. Turan, S. Yigit, and N. Chakraborty, *Numerical investigation of mixed convection of Bingham fluids in cylindrical enclosures with heated rotating top wall*, International Journal of Heat and Mass Transfer, 108, 1850 -1869(2017).

[15]A.N. Alexandrou, Ph.L. Menn, G. Georgiou, and V. Entov, *Flow instabilities of Herschel-Bulkley fluids*, J. Non-Newtonian Fluid Mech., 116, 19-32(2003).

[16]E. Mitsoulis, *Flows of viscoplastic materials: models and computations*, Rheology Reviews, 135-178(2007).

[17]H. Zhu, Y.D. Kim, and D. DeKee, *Non-Newtonian fluids with a yield stress*, J. Non-Newtonian Fluid Mech., 129, 177-181(2005).

[18]Z.M. Gharsseldien, Kh.S. Mekheimer, and A.S. Awad, *The influence of slippage on trapping and reflux limits with peristalsis through an asymmetric channel*, Applied Bionics and Biomechanics, 7(2), 95-108(2010).

[19]R.E.S. Abo Elkhair, *Lie point symmetries for amagneto couple stress fluid in a porous channel with expanding or contracting walls and slip boundary condition*, Journal of the Egyptian Mathematical Society, 24, 656-665(2016).

[20]T. Hayat, H. Zahir, A. Tanveer, and A. Alsaedi, *Influences of Hall current and chemical reaction in mixed convective peristaltic flow of Prandt lfluid*, Journal of Magnetism and Magnetic Materials, 407, 321-327(2016).

[21]N.T. Eldabe, A.S. Zaghrout, H.M. Shawky, and A.S. Awad, , *Peristaltic transport of micropolar fluid through porous medium in a symmetric channel with heat and mass transfer in the presence of generation and radiation*, African Journal of Mathematics and Computer Science Research, 6(6), 121-129(2013).

[22]M.M. Bhattia, and M.M. Rashidi,*Study of heat and mass transfer with Joule heating on magnetohydrodynamic (MHD) peristaltic blood flow under the influence of Hall effect*, Propulsion and Power Research, 6(3), 177-185(2017).

[23]M.M. Bhattia, M. Ali Abbas, and M.M. Rashid, *Combine effects of Magnetohydrodynamics (MHD) and partial slip on peristaltic Blood flow of Ree-Eyring fluid with wall properties*, Engineering Science and Technology, an International Journal, 19, 1497-1502(2016).

[24]N.T. Eldabe, M.A. Elogail, S.M. Elshaboury, and A.H. Alfaisal, *Hall effects on the peristaltic transport of Williamson fluid through a porous medium with heat and mass transfer*, Applied Mathematical Modelling, 40, 315-328(2016).

[25]T.C. Papanastasiou, *Flows of materials with yield*, J. Rheol., 31, 385-404(1987).

Nabil T. M. Eldabe received the B. S. in 1970 at the Department of Mathematics in Faculty of Education, Ain Shams University, Cairo, Egypt. Also, he received another B.S. in 1972 at the Department of Mathematics in Faculty of Science, Ain Shams University. Furthermore, he received M.S. degree from Girls College, Ain Shams University, in 1975. In1980, he received the PH.D. From Faculty of Science, Assiut University, Assiut, Egypt. From 1970 to 1974, he had been employed as demonstrator, from 1975 to 1979, he had worked as an assistant lecturer, from 1980 to 1984, he had worked as a lecturer, from 1985 to 1989 he had worked as an assistant professor and from 1990 to 2009, he had worked as a professor at Department of Mathematics, Faculty of Education, Ain Shams University. Also, from 1999 to 2005 and 2006 to 2009, he had been employed as head of the Department of Mathematics, Faculty of Education, Ain Shams Un. From 2007 to 2008, he had been employed as director for the Center of Development and Teaching Science at Ain Shams Un. From 2009 until now, he is emeritus professor in Faculty of Education, Ain Shams Un. Further, he had been employed as a head of the Department of Mathematics, Jouner College and Teachers College, Saudi Arabia from (1983 to 1988) and from (1994 to 1999). Also, he received Amin Loutfy prize, one of the Egyptian encouragements prizes in scientific fields (1989). He was teaching most of the mathematics curriculum in Saudi Arabia, the United Arab Emirates and participating in the conferences of the Hashemite Kingdom of Jordan.

Amira S. A. Asar received the B. S. in 2003 in Mathematics from Mathematics Department, Faculty of Science (Girls), Al-Azhar University, Cairo, Egypt. Furthermore, she received M. Sc degree in Applied Mathematics form Mathematics Department, Faculty of Science (Girls), Al-Azhar University in 2011. In 2015 she got the Ph.D. in Applied Mathematics form Mathematics Department, Faculty of Science (Girls), Al-Azhar University. From 2004 to 2011, she had been employed as demonstrator, from 2012 to 2015, she had been worked as an assistant lecturer at the Department of Mathematics in the Faculty of Science (Girls), Al-Azhar University. She has been worked as a lecturer at Mathematics Department, Faculty of Science (Girls), Al-Azhar University from 2015 until now. Her research field interested in the branches of applied mathematics especially Fluid mechanics.

Hameda M. Shawky is Associate professor of Applied Mathematics Faculty of Science (Girls) , Al-Azhar University, Cairo, Egypt. She received the PH.D. in Applied Mathematics at Department of Mathematics, Faculty of Science, Cairo University. Her research interests are in Hydrodynamics including Nano fluids. She has published several research articles in reputed international journals of applied Mathematics. She is referee of mathematical journals.